

# Electrophysiological, Morphological, and Topological Properties of Two Histochemically Distinct Subpopulations of Cerebellar Unipolar Brush Cells

Jin-Ah Kim · Gabriella Sekerková · Enrico Mugnaini · Marco Martina

Published online: 14 April 2012  
© Springer Science+Business Media, LLC 2012

**Abstract** Unipolar brush cells (UBCs) are excitatory cerebellar granular layer interneurons whose brush-like dendrites receive one-to-one mossy fiber inputs. Subclasses of UBCs differ primarily by expressing metabotropic glutamate receptor (mGluR) 1 $\alpha$  or calretinin. We used GENSAT Tg(Grp-EGFP) BAC transgenic mice, which selectively express enhanced green fluorescent protein (EGFP) in mGluR1 $\alpha$ -positive UBCs to compare the functional properties of the two subclasses. Compared to EGFP-negative UBCs, which include the calretinin-positive cells, EGFP-positive UBCs had smaller somata (area 48 vs 63  $\mu\text{m}^2$ ), lower specific membrane resistance (6.4 vs. 13.7  $\text{K}\Omega \text{cm}^2$ ), were less prone to intrinsic firing, and showed more irregular firing (in cell-attached ~49 % were firing vs. ~88 %, and the CV was 0.53 vs. 0.32 for EGFP-negative cells). Some of these differences are attributable to higher density of background  $\text{K}^+$  currents in EGFP-positive cells (at  $-120 \text{ mV}$ , the barium-sensitive current was 94 vs. 37 pA in EGFP-negative cells);  $I_h$ , on the contrary, was

more abundantly expressed in EGFP-negative cells (at  $-140 \text{ mV}$ , it was  $-122$  vs.  $-54 \text{ pA}$  in EGFP-positive neurons); furthermore, while group II mGluR modulation of the background potassium current in EGFP-negative UBCs was maintained after intracellular dialysis, mGluR modulation in EGFP-positive UBCs was lost in whole-cell recordings. Finally, cell-attached firing was reversibly abolished by the  $\text{GABA}_B$  activation in EGFP-positive, but not in EGFP-negative UBCs. Immunohistochemistry showed that EGFP-negative UBCs express GIRK2 at high density, while mGluR1 $\alpha$  UBCs are GIRK2 negative, suggesting that GIRK2 mediates the mGluR-sensitive current in EGFP-negative UBCs. These data suggest that the two subclasses perform different functions in the cerebellar microcircuits.

**Keywords** Calretinin ·  $\text{GABA}_B$  · GIRK · mGluR1 $\alpha$  · Modulation · Vestibulocerebellum

J.-A. Kim · E. Mugnaini · M. Martina (✉)  
Department of Physiology, Northwestern University,  
Feinberg School of Medicine,  
303 E. Chicago Avenue,  
Chicago, IL 60611, USA  
e-mail: m-martina@northwestern.edu

G. Sekerková · E. Mugnaini  
Department of Cell and Molecular Biology,  
Northwestern University, Feinberg School of Medicine,  
Chicago, IL 60611, USA

G. Sekerková · E. Mugnaini  
Knowles Hearing Center, School of Communication,  
Northwestern University,  
2240 Campus Drive North,  
Evanston, IL 60208, USA

## Introduction

The cerebellar unipolar brush cells (UBCs) and the granule cells are the only excitatory glutamatergic interneurons of the cerebellar cortex [1, 2]. UBCs are particularly enriched in the granular layer of the vestibulocerebellum and the vermis, where they receive one-to-one afferent inputs from vestibular mossy fibers [3, 4]. Based on chemical properties [1, 5, 6] and time of origin [7], UBCs are classified into two main subclasses. The major UBC subclass, which makes up approximately two thirds of the population, is represented by cells expressing the metabotropic glutamate receptor subtype mGluR1 $\alpha$  (mGluR1 $\alpha^+$ ), and the second subclass by cells expressing the calcium binding protein calretinin (CR+) [1].

Basic electrophysiological properties set UBCs apart from neighboring cells. In particular, input resistance and capacitance are very different from either Golgi or granule cells [8–11]. The firing properties, arguably the single most important neuronal electrophysiological parameter as it determines the neuronal signal transfer function, also distinguish UBCs from neighboring granule cells, although differences exist in the published data concerning the UBC firing phenotype. In particular, *in vitro* studies showed the UBCs to be either T-type calcium current-dependent bursting cells that are mostly silent at rest [12] or intrinsically spiking neurons that fire at low, regular frequency [10, 11]. *In vivo* recordings also found that UBCs may be either regularly firing at 10–30 Hz or bursting [13, 14]. Although no other morphological or functional differences have been identified between the two UBC subtypes so far, it could be suggested that the different electrophysiological properties attributed to UBCs in general may correspond to recordings from one or the other of two distinct neuronal subclasses. By taking advantage of gastrin-releasing peptide enhanced green fluorescent protein (Grp-EGFP) BAC transgenic mice (Tg(Grp-EGFP)DV197Gsat) [15], in which the green fluorescent marker (EGFP) is expressed in the mGluR1 $\alpha$ + UBCs, this study shows that murine UBCs consist of two subsets of cells with different somatic size and functional properties. We show that the CR+ UBCs are larger, intrinsically and regularly firing, electronically tighter, express relatively large Ih, and have GIRK2 channels that are modulated by group II mGluRs even after intracellular dialysis. The EGFP-positive (mGluR1 $\alpha$ +) UBCs are depolarized by group I mGluR activation, have smaller soma size, show bursting phenotype, and low Ih expression; they also display larger background potassium currents that are not mediated by GIRK2 subunits and are modulated by GABA<sub>B</sub> and group II mGluR activation but only in intact cell recordings. The possible functional consequences of these differences are discussed.

## Materials and Methods

**Animals** This study was carried out on mice in accordance with the guidelines issued by the National Institutes of Health and the Society for Neuroscience to minimize the number of animals used and their suffering.

Tg(Grp-EGFP)DV197Gsat mice generated by the GENSAT project [15, 16] were obtained from Drs. J.P. Doyle, J.D. Dougherty and N. Heintz (Rockefeller University, New York, NY, USA). The animals were bred and housed in the barrier-level mouse vivarium in the Center for Comparative Medicine at Northwestern University Feinberg School of Medicine. Multiple cycles of random mating within the subcolony, without the re-introduction of exogenous breeders, produced a

closed subline in which transgene expression was largely restricted to the cerebellum and the cochlear nuclear complex. Genomic DNAs obtained from ear punches were tested by PCR using EGFP forward primer 5'-CCT ACG GCG TGC AGT GCT TCA GC-3' and reverse primer 5'-CGG CGA GCT GCA CGC TGC GTC CTC-3' (IDT). Mice positive for the transgene were mated to each other. Homozygous and heterozygous animals were used in the experiments, and adult mice negative for the transgene were used as controls. In both homozygous and heterozygous mice, EGFP was expressed in the UBCs. EGFP-positive and EGFP-negative mice at postnatal day 28 (P28) and P60 were used for histological evaluation and quantification, while EGFP-positive P21–35 mice were used for electrophysiological recording.

**Immunohistochemistry** Deeply anesthetized mice (sodium pentobarbital, 60 mg/kg body weight) were perfused through the ascending aorta with 4 % freshly depolymerized paraformaldehyde in 0.12 M phosphate buffer. The cerebella were dissected out and were either embedded in paraffin or cryoprotected for cryosectioning. Sagittal or coronal cerebellar sections from the paraffin-embedded blocks were cut at 8  $\mu$ m, deparaffinized in xylenes, and rehydrated in descending series of ethyl alcohols. Sections were subjected to antigens retrieval, using a pressure cooker with a 1 $\times$  Rodent Decloacker solution (Biocare Medical) at 125  $^{\circ}$ C for 20 min followed by a 10-min treatment with 0.1 % sodium borohydride in Tris-buffered saline (TBS; 100 mM Tris, 150 mM NaCl; pH 7.4). Cryoprotected cerebella were sectioned serially in the sagittal or coronal planes at 24  $\mu$ m on a freezing-stage microtome and collected in multiwell plates.

For immunohistochemistry in bright field microscopy, sections were processed for immunohistochemistry according to an avidin/biotin amplification protocol. Briefly, the endogenous peroxidase activity was blocked in 0.3 % H<sub>2</sub>O<sub>2</sub> and 10 % methanol in TBS, and unspecific binding was suppressed in a blocking solution containing 5 % normal goat serum (NGS) and 1 % bovine serum albumin (BSA) in TBS with 0.2 % Triton X-100. Sections were then incubated with primary antibodies overnight or up to 2 days at 4  $^{\circ}$ C. Bound antibodies were detected using biotinylated anti-mouse or anti-rabbit IgG (GE Healthcare), ABC Elite kit (Vector), and diaminobenzidine (Sigma). For immunofluorescence, sections were blocked with 5 % NGS and 1 % BSA in TBS with 0.2 % Triton X-100 followed by incubation with the primary antibodies. Bound primary antibodies were visualized by secondary antibodies coupled to Alexa 488 or Alexa 594 (Invitrogen).

For this study, we used the following primary antibodies: mouse anti-CR (1:1,000; Millipore or 1:2,000; Swant), rabbit anti-CR (1:5,000; Swant), mouse anti-EGFP (1:1,000; Millipore), rabbit anti-EGFP (1:5,000; Invitrogen), rabbit anti-GIRK2 (Kir3.2; 1:200; Alomone or 1:100–500; Millipore), mouse anti-mGluR1 $\alpha$  (1:800–1,000; Pharmingen

or 1:150; Histopathology Ltd., Hungary), rabbit anti-mGluR1 $\alpha$  (1:1500; from Dr. R. Shigemoto, SORST-JST, Myodaiji, Okazaki, Japan), and rabbit anti-Tbr2 (1:2,000; from Dr. R.F. Hevner, University of Washington, Seattle, WA, USA). Specificity of the antibodies was confirmed by the absence of immunoreaction signal in control sections incubated without primary antibodies (data not shown).

Immunofluorescence images of cerebellar sections were acquired with a Spot RT CCD video camera (Diagnostic Instruments) mounted on a Nikon Eclipse E800 microscope. Laser scanning confocal images were obtained with a Nikon PCM 2000 Confocal Microscope System using Simple PCI Program. Images were analyzed individually or in z-stacks of different depths. For co-localization experiments, type DF immersion oil (Fryer) was used with either a  $\times 40$  plan-fluor lens (numerical aperture 1.3) or a  $\times 60$  plan-apochromatic lens (numerical aperture 1.4). To minimize channel spillover, the images were sequentially acquired. All images were processed with Adobe Photoshop CS2. Brightness and contrast were adjusted.

**Cell Size Measurements** The cell body sizes of mGluR1 $\alpha$ + UBCs and CR+ UBCs were measured in neighboring sections double-stained with antibodies recognizing mGluR1 $\alpha$  and EGFP or CR and EGFP, respectively. Confocal z-stack images of UBCs localized in lobules IX and X were taken with oil immersion objective lenses at  $40\times 3$  (CR) and  $60\times 3$  (mGluR1 $\alpha$ ) magnification. A total of 250 mGluR1 $\alpha$ + UBC and 250 CR+ from five mice (50 cells/each animal) were measured. Only cells with a brush and a soma within the same plane (within  $\sim 5$   $\mu\text{m}$  depth) were used for measurements. Tiff images were transferred to NIH ImageJ program (available on the Internet at <http://rsb.info.nih.gov/ij/>), where the UBC somata were outlined using the free-hand selection tool. The outlined area was automatically calculated by ImageJ program. Data were analyzed using InStat 3.0 (GrapPad Software).

**Electrophysiological Recordings** Homozygous and heterozygous Tg(Grp-EGF) mice were deeply anesthetized with isoflurane (0.3 ml in 1,000 ml administered for  $\sim 90$  s) and killed by decapitation. The cerebella were quickly ablated and placed in ice-cold modified artificial cerebrospinal fluid containing (in millimolars): 125 NaCl, 25 NaHCO<sub>3</sub>, 2.5 KCl, 1.25 NaH<sub>2</sub>PO<sub>4</sub>, 0.2 CaCl<sub>2</sub>, 7 MgCl<sub>2</sub>, and 25 glucose and 2 kynurenic acid, saturated with 95 % O<sub>2</sub> and 5 % CO<sub>2</sub>. Parasagittal slices, 300  $\mu\text{m}$  thick, were cut from the median cerebellum using a vibrating blade microtome (Microm). Slices were incubated in a sucrose-rich solution containing (in millimolars): 87 NaCl, 25 NaHCO<sub>3</sub>, 2.5 KCl, 1.25 NaH<sub>2</sub>PO<sub>4</sub>, 0.5 CaCl<sub>2</sub>, 7 MgCl<sub>2</sub>, 75 sucrose, and 25 glucose, bubbled with 95 % O<sub>2</sub> and 5 % CO<sub>2</sub> for 20–30 min at 35 °C and then at room temperature. For electrophysiological

measurements, slices were transferred to a recording chamber at room temperature and were visualized with an Axioskop FS (Zeiss) upright microscope using infrared differential interference contrast videomicroscopy under a water-immersion  $\times 40$  objective lens. During recordings, slices were continuously superfused with physiological extracellular solution containing (in millimolars): 125 NaCl, 25 NaHCO<sub>3</sub>, 2.5 KCl, 1.25 NaH<sub>2</sub>PO<sub>4</sub>, 1.5 CaCl<sub>2</sub>, 1 MgCl<sub>2</sub>, and 25 glucose, saturated with 95 % O<sub>2</sub> and 5 % CO<sub>2</sub>. All recordings were performed from lobule IX and lobule X. EGFP-tagged UBCs were identified using epifluorescence illumination (X-cite, Mississauga, ON, Canada). EGFP-negative UBCs included all the CR+ UBCs and an undetermined proportion of the mGluR1 $\alpha$ + UBCs. EGFP-negative UBCs were visually selected based on size and shape. Typically, EGFP-negative UBCs had a capacitance of  $21.2\pm 0.74$  pF, much larger than granule cells [10] and smaller than Golgi cells [8, 9]; their identification as UBCs was confirmed by observation of the characteristic brush upon intracellular dialysis with the fluorescent dye Alexa-fluor 488 (1 mg/ml) or Lucifer yellow (1 mg/ml). The presence of intrinsic firing was tested in cell-attached configuration in the presence of 2 mM kynurenic acid, 100  $\mu\text{M}$  picrotoxin, and 1  $\mu\text{M}$  strychnine to block fast synaptic transmission.

Pipettes were pulled from Dagan SG16 glass (OD 1.65 mm; ID 0.75 mm) using a horizontal puller (P97, Sutter). For whole-cell recordings, pipettes were filled with internal solution consisting of (in millimolars): K-gluconate 130, NaCl 10, MgCl<sub>2</sub> 2, EGTA 0.1, Na<sub>2</sub>ATP 2, NaGTP 0.1, and HEPES 5, pH 7.3 with KOH. Pipette tip resistances in working solutions ranged from 5 to 8 M $\Omega$  yielding series resistances of  $<50$  M $\Omega$  that were compensated 40 to 60 %. For cell-attached recordings, the resistance of the pipettes was in the same range as used for whole-cell recordings. The internal solution for cell-attached recordings was extracellular HEPES-buffered ACSF (1.5 mM [Ca<sup>2+</sup>]<sub>o</sub>) for the recordings shown in Figs. 2, 10 and 11, and it was K-gluconate for data in Fig. 6.

All recordings were performed at 22–24 °C using an Axopatch 200B amplifier (Axon Instruments). Current signals were low-pass filtered at 2 or 5 KHz (four-pole low-pass Bessel filter on amplifier) and digitized (10 KHz) using a Digidata 1321A controlled by pClamp8 software interface (Axon instruments). Signals from current-clamp recordings were sampled at 20 KHz and filtered at 10 KHz.

Drugs and chemicals were from Sigma, except picrotoxin, DHPG, APDC, baclofen, CGP55845, and t-ACPD that were from Tocris; they were bath applied. All recorded cells were filled for post hoc anatomical examination. At the end of the recording, slices were fixed in 4 % paraformaldehyde in 0.1 MPB for 24 h. After fixation, slices were rinsed in PB several times. Finally,



slices were coverslipped with Mowiol (Aldrich)-based antifading mounting medium.

**Statistical Analysis** Comparisons between different samples were performed using ANOVA; comparisons of individual cells before and after treatment were performed using paired *t* tests. Statistical significance was evaluated at the level of  $p < 0.05$ . All data are expressed as mean and SEM. Error bars in the figures also represent SEM.

**Multivariate Analysis** Principal component analysis [17] was performed using commercially available software (MVSP). Data were standardized into *z* scores and the four variables reduced to two dimensions. The two axes accounted for >80 % of the total sample variance. For cluster analysis, a similarity matrix between each pair of cases was calculated. The hierarchical dendrogram was then constructed using a minimum variance algorithm.

## Results

To validate the expression pattern of the cellular markers mGluR1 $\alpha$ , CR, and EGFP in our closed, Tg(Grp-EGFP) mouse subcolony, cerebellar sections of homozygous and heterozygous transgenic mice were analyzed by single and double-immunofluorescence with antibodies of proven specificity.

Immunohistochemistry in adult mice with antibodies to EGFP, mGluR1 $\alpha$ , and CR using an immunoperoxidase staining confirmed that the lobular distribution of EGFP-positive neurons throughout the cerebellar cortex in general (data not shown) and in lobules IX and X in particular (Fig. 1a–c) was fully congruent with that of the mGluR1 $\alpha$ + UBCs. Additionally, every EGFP-positive neuron tested responded to application of the type I mGluR agonist DHPG (50  $\mu$ M, eight cells) with an increase in firing frequency (Fig. 2). The regional positioning of the EGFP-positive UBCs did not match, albeit it partially overlapped, that of the CR+ UBCs (compare Fig. 1a with c). At the single-cell level, EGFP immunoreactivity appeared more intense in the cell body than in the dendritic compartment (Figs. 1a' and 3a, d, g) and was usually absent from the axon (Fig. 1a'), except in the initial segment (data not shown). The identification of EGFP-positive neurons with the mGluR1 $\alpha$ + UBCs (Fig. 3a–c) was unmistakable, in spite of the fact that the brushes were faintly EGFP immunoreactive and intensely mGluR1 $\alpha$ + while the cell bodies distinctly EGFP immunoreactive and only faintly mGluR1 $\alpha$ + (see also Fig. 1a', b'). By contrast, the CR+ UBCs appeared intensely immunoreactive in the entire somatodendritic compartment (Figs. 1c' and 3e, f) and in the axonal compartment (data not shown), as previously demonstrated [1, 18, 19]. The

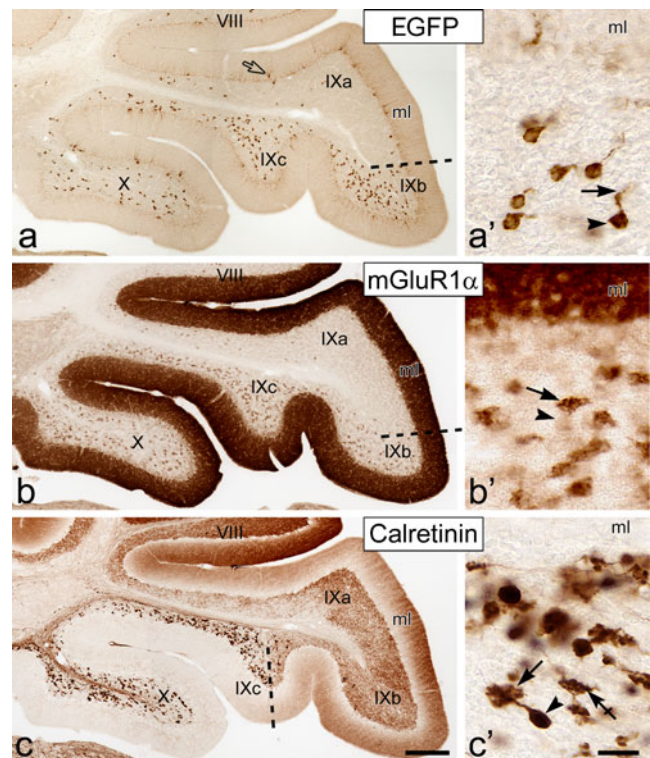


**Fig. 1** Distribution of UBC subclasses in the Tg(Grp-EGFP) BAC transgenic mice cerebellum. Images from parasagittal cryosections immunoreacted with antibodies to EGFP, mGluR1 $\alpha$ , and CR (as indicated) show the two lobules (lobule X—the nodulus and vermal lobule IX—the uvula) that contain the highest UBC densities. *a–c* Dash lines mark the border of the region enriched with EGFP-positive, mGluR1 $\alpha$ +, and CR+ UBCs. The distributions of EGFP-positive and mGluR1 $\alpha$ + UBCs are in register and overlap only partially with the CR+ UBCs. There is slight expression of EGFP in the Golgi–Bergmann glia (open arrow in *a*) as previously reported. In the molecular layer (*ml*), strong mGluR1 $\alpha$  immunoreactivity is localized to the Purkinje cell dendrites (*b*), whereas CR immunoreactivity is localized to ascending granule cell axons and their parallel fibers (*c*). *a'–c'* Higher magnification images of UBCs from lobule X showing differential immunostaining of the UBC soma (arrowhead) and brush (arrow) with antibodies to EGFP (*a'*), mGluR1 $\alpha$  (*b'*), and calretinin (*c'*). Crossed-arrow in *c'* indicates CR+ mossy fiber terminal. Scale bars: *a–c* 200  $\mu$ m; *a'–c'*, 20  $\mu$ m

CR+ UBCs were not immunolabeled by EGFP antisera (Fig. 3d–f). Double labeling with antibodies to EGFP and Tbr2 (a marker for the entire UBC population [20, 21]) further confirmed that all EGFP-labeled cells were UBCs (Fig. 3g). In the EGFP-positive UBCs, the nucleoli were usually densely stained (Fig. 3a, d, g), and in some UBCs, nuclear infoldings were also detectable (Fig. 3a).

EGFP expression highlighted the cell body of mGluR1 $\alpha$ + UBCs and generated the overall visual impression that the EGFP/mGluR1 $\alpha$ -immunoreactive UBCs have smaller soma size than the CR+ UBCs (compare Figs. 1a' and 3c with Figs. 1c' and 3f, respectively). To validate this difference, we measured the cell bodies of 250 UBCs in each of the two subclasses after immunostaining with anti-EGFP paired with

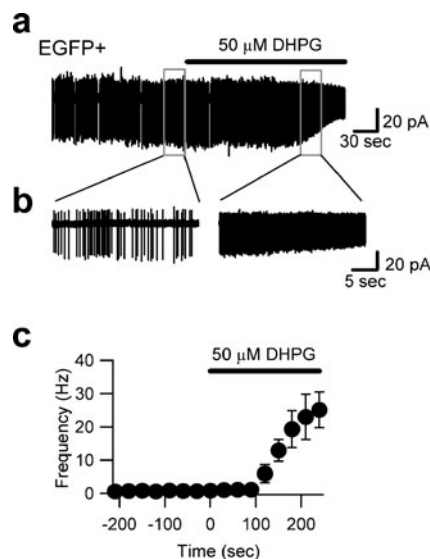


**Fig. 2** Group I mGluR activation depolarizes EGFP-positive UBCs. **a** Cell-attached recording from a EGFP-positive cerebellar UBC in an acute mouse slice in the presence of blockers of fast synaptic transmission. Type I mGluR agonist DHPG increased the frequency of intrinsic firing, while decreasing the spike amplitude, in keeping a depolarizing effect. The trace segments within the *boxes* are shown on an enlarged time-scale in **b**. **c**, Summary of the effect of DHPG on the firing frequency of eight neurons

anti-mGluR1 $\alpha$  or anti-CR. As shown in Fig. 3h, the average somatic area of EGFP-immunoreactive mGluR1 $\alpha$ + UBCs was  $48.3 \pm 0.4 \mu\text{m}^2$  (range 33.1 to  $66.4 \mu\text{m}^2$ ), while it was  $63.2 \pm 0.6 \mu\text{m}^2$  (range 42.4 to  $83.3 \mu\text{m}^2$ ) for CR+ UBCs ( $p < 0.05$ ).

The intensity of EGFP expression varied among UBCs. Strong EGFP signal was easily detectable by standard fluorescence microscopy, while low signal required confocal microscopy (Fig. 3g). Notably, the proportion of intensely fluorescent UBCs was higher in presumed homozygotes than in heterozygotes as previously reported [15] although it never encompassed the entire mGluR1 $\alpha$ + UBC population. To ascertain that EGFP was indeed expressed by mGluR1 $\alpha$ + UBC, we analyzed coexpression of the two proteins in confocal images. We found that 99.9 % of EGFP expressing UBCs were labeled by mGluR1 $\alpha$  antiserum; out of 1,098 EGFP-positive cells ( $N=3$  mice), only two UBCs were mGluR1 $\alpha$ -.

In Tg(Grp-EGFP) mice, mGluR1 $\alpha$ + UBCs and CR+ UBCs formed two largely non-overlapping populations (data not shown) as previously reported in adult CD1 mice [1]. UBCs immunoreactive for both cellular markers were extremely rare, in agreement with previous studies in rat and other mammals [2, 20], although the number of such cells was slightly more frequent in P22–24 TG (Grp-EGFP) mice than in the adults, presumably as a consequence of the still ongoing maturation process; however, the number of such neurons was still negligible (3–5 %; data not shown). Moreover, the rare

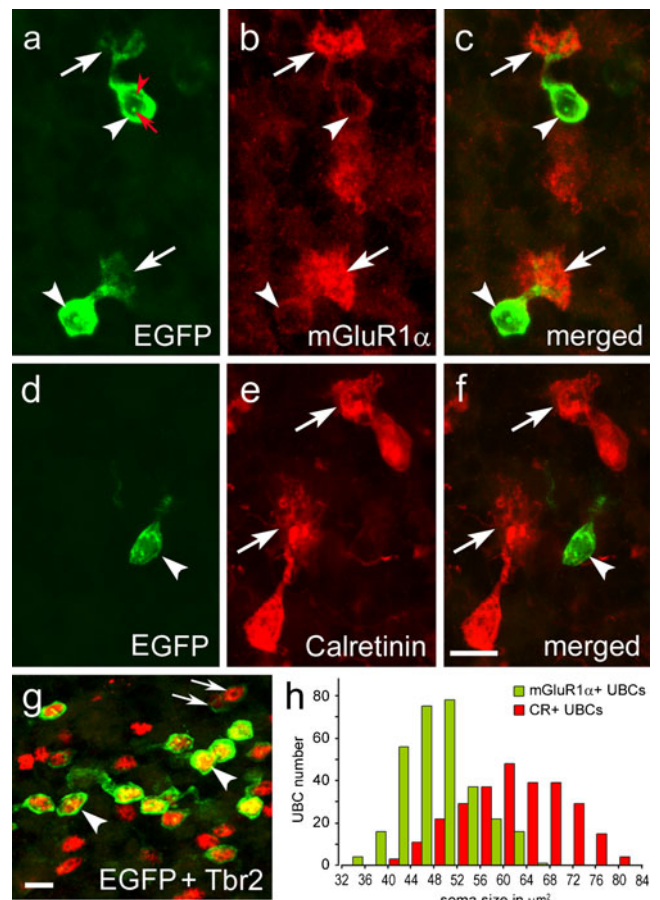


**Fig. 3** Immunofluorescence of chemically distinct UBC subclasses in the cerebellum of Tg(Grp-EGFP) BAC transgenic mice. **a–g** Confocal images from two-color immunolabeled cryosections. EGFP-positive UBCs are mGluR1 $\alpha$ + (**a–c**), but CR-negative (**d–f**). In **a–f**, *arrowheads* indicate cell bodies and *arrows* point to brushes; the nucleoli of EGFP-positive UBCs are conspicuously labeled (*red arrow*) and a nuclear infolding is labeled by *red arrowhead*. EGFP is intensely expressed in many UBCs labeled by Trb2 (*arrowhead*); faintly EGFP-positive UBCs are indicated by *arrows* (**g**). **h** Bar graph illustrates cell subclass differences in the soma size of mGluR1 $\alpha$ + and CR+ UBCs. Scale bars: **a–g** 10  $\mu\text{m}$

EGFP/CR double-labeled UBCs were only faintly EGFP immunofluorescent (not shown), in contrast to the single-labeled (EGFP-positive) UBCs, which showed intense fluorescence labeling. The data indicated that Tg(Grp-EGFP) mice can be advantageous to reliably identify one of the two UBC subsets in fresh slices and determine its electrophysiological properties, as a step toward the functional definition of both UBC subtypes.

The electrophysiological phenotype of the two neuronal populations was studied using patch clamp recordings in acute slices. For these experiments, we used 21–35-day-old mice and we selected UBCs that displayed either an unmistakable intrinsic fluorescence or lacked fluorescent signal altogether, with the caveat that a small number of the latter may represent mGluR1 $\alpha$ + UBCs (for more details,

see “Materials and Methods” and data discussed in Fig. 13). The recordings were performed in the presence of blockers of fast synaptic transmission (2 mM kynurenic acid, 100  $\mu$ M picrotoxin, and 1  $\mu$ M strychnine). Cells belonging to the two groups showed different response to injection of negative and positive currents (Fig. 4a, b). In keeping with the anatomical analysis showing different cell size, EGFP-positive and EGFP-negative UBCs had different capacitance ( $16.6\pm 0.7$  and  $20.2\pm 0.7$  pF,  $n=51$  and 42, respectively,  $p<0.05$ ; Fig. 4c); the input resistance also differed (it was  $6.4\pm 0.5$  and  $13.7\pm 0.9$   $k\Omega\text{ cm}^2$ , respectively,  $p<0.05$ ; Fig. 4d), suggesting a differential expression of background current between the two cell types.

Current-clamp recordings in response to injection of hyperpolarizing currents showed that the amplitude of the membrane potential “sag” elicited by hyperpolarizations

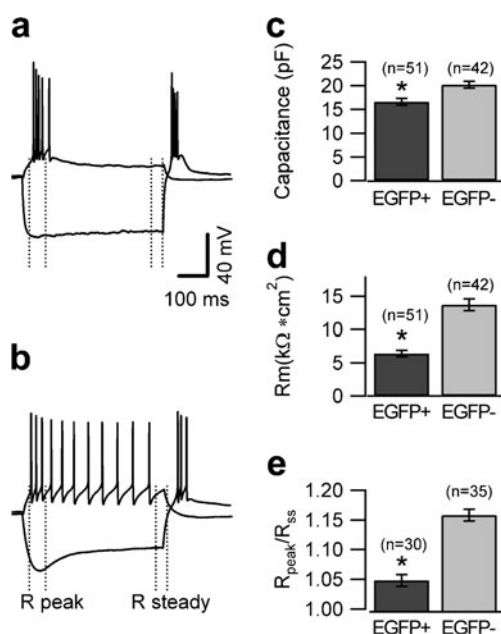


**Fig. 4** Distinctive intrinsic properties of EGFP-positive and EGFP-negative UBCs. **a, b** Voltage recordings from one EGFP-positive (**a**) and one EGFP-negative (**b**) UBC in response to 500-ms-long injections of hyperpolarizing ( $-220$  pA for EGFP-positive UBC and  $-80$  pA for EGFP-negative UBC) and depolarizing current ( $40$  pA for EGFP-positive UBC and EGFP-negative UBC). The injected hyperpolarizing current was tuned to produce equal peak voltage responses ( $-130$  mV) in the two cells. The *dotted lines* indicate the trace segments used for the determination of peak and steady-state input resistance. **c** Bar chart comparing the value of the capacitance in two cell types. Capacitance values were  $16.6\pm 0.7$  pF in EGFP-positive and  $20.2\pm 0.7$  pF in EGFP-negative UBCs ( $n=51$  and 42, respectively,  $p<0.05$ ). **d** Bar chart comparing the value of the specific membrane resistance in two cell types. Specific resistance was determined assuming specific membrane capacitance of  $1\text{ }\mu\text{F}/\text{cm}^2$ . EGFP-positive UBCs have lower specific resistance than EGFP-negative UBCs ( $6.4\pm 0.5$  and  $13.7\pm 0.9$   $k\Omega\text{ cm}^2$ ,  $n=51$  and 42, respectively,  $p<0.05$ ). **e** Bar chart showing the ratio of the peak to steady-state input resistance in the two cell types. The ratio was  $1.16\pm 0.01$  in EGFP-negative UBCs and  $1.05\pm 0.01$  in EGFP-positive UBCs ( $n=35$  and 30, respectively,  $p<0.05$ )

from  $-70$  to  $-130$  mV was larger in EGFP-negative than in EGFP-positive UBCs. The ratio of the peak to steady-state input resistance was  $1.16\pm 0.01$  in EGFP-negative and  $1.05\pm 0.01$  in EGFP-positive UBCs ( $n=35$  and 30, respectively,  $p<0.05$ ; Fig. 4a, b, e). Voltage-clamp recordings were then performed to better characterize this difference. Hyperpolarization-activated currents were recorded in control condition and in the presence of the  $I_h$  blocker ZD7288 ( $100\text{ }\mu\text{M}$ ); in keeping with the current-clamp data, the size of  $I_h$  was larger in EGFP-negative neurons ( $-121.9\pm 34.6$  vs.  $-53.7\pm 8.4$  pA at  $-140$  mV;  $p<0.05$ , Fig. 5c). No differences were found in the voltage dependence of  $I_h$  activation between the two UBC subtypes (Fig. 5d)

The firing phenotype, recorded in the whole-cell configuration, also differentiated the two cell populations (Fig. 6). EGFP-positive UBCs showed bursting behavior and in 63 % of the cases were silent without current injection ( $V_m$  was  $-60.5\pm 0.8$  mV,  $n=32$ , Fig. 6a, e), partly resembling the phenotype described by Diana et al. [12] in rat slices, while the vast majority of EGFP-

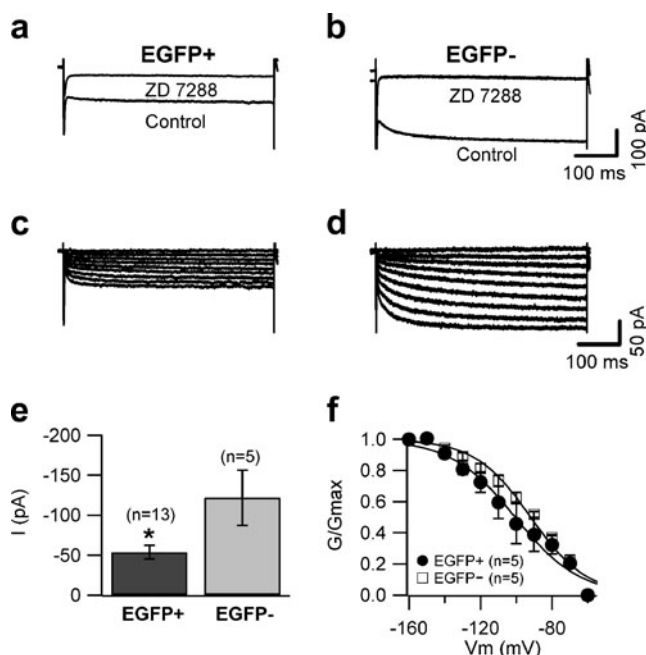


**Fig. 5** Differential  $I_h$  expression in EGFP-positive and EGFP-negative UBCs. Representative traces of currents recorded in EGFP-positive (**a**) and EGFP-negative (**b**) UBCs in response to 500-ms-long voltage steps in control conditions and after bath application of  $100\text{ }\mu\text{M}$  ZD7288 (at  $-140$  mV). **c, d** Traces of the ZD7288-sensitive current obtained by digital subtraction. Cells were held at  $-60$  mV and clamped at potentials between  $-60$  and  $-160$  mV in  $10$  mV steps. The *bar chart* in **e** represents the size of ZD7288-sensitive currents (at  $-140$  mV) in EGFP-positive and EGFP-negative UBCs;  $I_h$  was larger in EGFP-negative UBCs. **f** Conductance–voltage relationship of the ZD7288-sensitive current. The data points were fit with a Boltzmann equation. Half points and slopes of the fits were not statistically different between the two populations



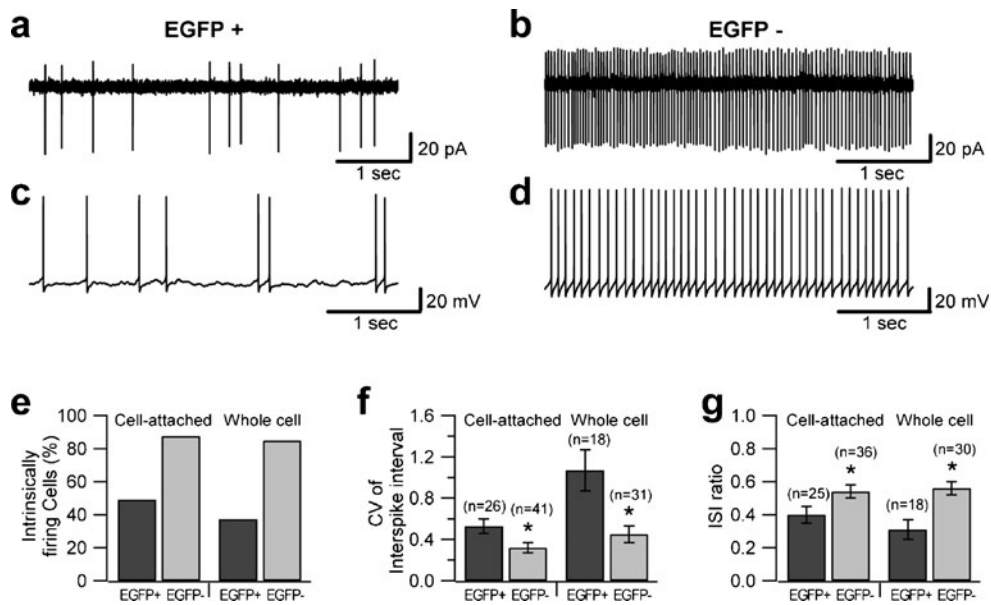


**Fig. 6** Intrinsic firing patterns differ in EGFP-positive and EGFP-negative UBCs. **a–d** Voltage-clamp cell-attached recordings (**a, b**) and whole-cell current-clamp recordings (**c, d** no current injection) of intrinsic firing in UBCs. EGFP-positive cells (**a, c**) exhibited spontaneous bursting, while EGFP-negative cells (**b, d**) fired more regularly. **e** Bar chart summarizing the fraction of intrinsically firing cells in the two populations: 88 and 85 % of EGFP-negative UBCs were intrinsically firing in cell-attached (48 total recordings) and whole-cell recording (40 total recordings), respectively. For EGFP-positive UBCs, the fraction of intrinsically firing cells was 49 % in cell-attached recording

and 37 % in whole-cell recording (55 and 51 recordings, respectively). **f** Coefficient of variation of the interspike interval in the two cell types. In the cell-attached recording, the values were 0.53 for EGFP-positive UBCs and 0.32 for EGFP-negative UBCs. In whole-cell recording, the values were 1.07 for EGFP-positive UBCs and 0.45 in EGFP-negative UBCs ( $p < 0.05$ ). **g** Interspike interval ratio (obtained by dividing the shortest interspike interval in the recording by the average interspike interval) measured in cell-attached recording and whole-cell recording in the two UBC subpopulations

negative cells (85 %, in whole-cell recordings) were spontaneously and regularly firing (Fig. 6b, d, e), similar to what previously reported in wild-type mice by Russo et al. [10]. The diverse firing pattern of the two populations was apparent in the coefficient of variation of the instantaneous firing frequency (CV), which was considerably higher in EGFP-positive UBCs. In whole-cell recordings, the CV was  $1.07 \pm 0.2$  for EGFP-positive cells and  $0.45 \pm 0.08$  for EGFP-negative cells ( $n = 18$  and  $31$ ; Fig. 6f;  $P < 0.05$ ). Intracellular dialysis might affect the delicate conductance equilibrium that controls action potential generation; therefore, the presence and regularity of intrinsic firing was also studied using extracellular recordings (cell-attached) to avoid interfering with the intracellular milieu. In this configuration, the results were similar to those in whole cell; 49 % of the EGFP-positive and 88 % of the EGFP-negative UBCs were spontaneously firing, and the CVs were  $0.53 \pm 0.07$  and  $0.32 \pm 0.03$ , respectively ( $n = 26$  and  $41$ ;  $p < 0.05$ , Fig. 6e, f).

What could be the mechanism underlying the different input resistances in the two populations? We previously showed that intrinsic UBC firing is regulated by group II mGluR receptor-coupled inward rectifier potassium currents [10]. Thus, we hypothesized that the differences between the properties of the two cell types could be mediated, at least in

part, by differential expression of these channels. To test this hypothesis, we compared the effect of extracellular barium (0.5 mM), a broad spectrum blocker of inward rectifier currents, in the two cell populations. Figure 7 shows that the barium-sensitive current was larger in EGFP-positive UBCs (at  $-120$  mV, the current was  $-93.9 \pm 15.1$  and  $-36.9 \pm 12.6$  pA in EGFP-positive and negative UBCs, respectively, six cells in each group,  $p < 0.05$ ; Fig. 7d). Accordingly, the effect of barium on the input resistance was larger in EGFP-positive cells (3- vs. 2-fold in EGFP-negative cells, Fig. 7e), supporting the hypothesis that background potassium channels, whose identity still needs to be characterized, are more prominently expressed in EGFP-positive cells. Interestingly, barium (0.5 mM, in the bath) appeared to act more slowly in EGFP-negative cells (not shown); the most conservative explanation for the slow onset of the effect is that the saturating barium concentration is lower in EGFP-positive than in EGFP-negative UBCs. In keeping with this hypothesis, 30  $\mu$ M barium blocked  $72.8 \pm 6.7$  % of the current blocked by 0.5 mM barium in EGFP-positive cells, but only  $47 \pm 6.3$  % in EGFP-negative cells (six cells in each group,  $p < 0.05$ ; Fig. 8), suggesting that the background currents in the two cell types differ not only in density but also in their molecular composition.

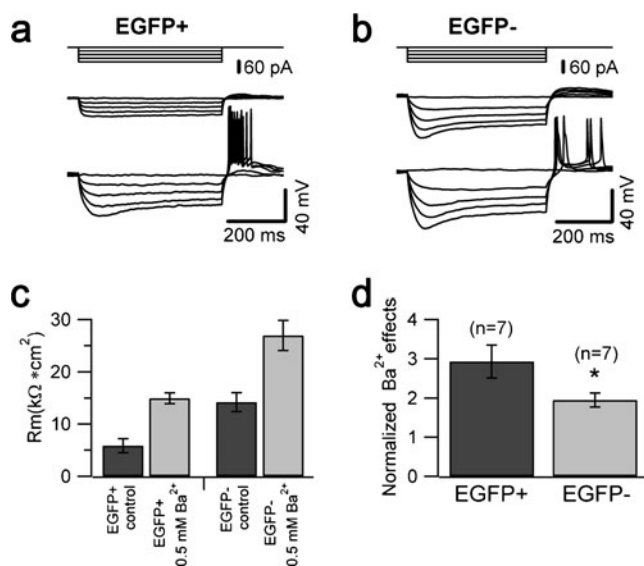


**Fig. 7** Differential effects of Ba<sup>2+</sup> on EGFP-positive and EGFP-negative UBCs. **a, b** Voltage traces recorded in an EGFP-positive (**a**) and an EGFP-negative UBC (**b**) in response to 500-ms-long hyperpolarizing current injections (from 0 to -80 pA, 20 pA steps, *upper traces*) in control conditions (*middle traces*) and after bath application of Ba<sup>2+</sup> (*lower traces*). **c** Bar chart summarizing the effect of 0.5 mM Ba<sup>2+</sup> on membrane resistance in EGFP-positive and EGFP-negative UBCs ( $n=7$ ). Specific membrane resistance in EGFP-positive UBCs was  $5.86 \pm 1.33$  kΩ cm<sup>2</sup> in control condition ( $n=7$ ) and increased following Ba<sup>2+</sup> application ( $14.95 \pm 1.05$  kΩ cm<sup>2</sup>), whereas resistance was increased from  $14.21 \pm 1.82$  kΩ cm<sup>2</sup> (control condition,  $n=7$ ) to  $26.97 \pm 2.89$  kΩ cm<sup>2</sup> (Ba<sup>2+</sup> application) in EGFP-negative UBCs. **d** Bar chart of the fractional effect of Ba<sup>2+</sup> on the specific membrane resistance in each cell type. The fractional effect of Ba<sup>2+</sup> was significantly larger in EGFP-positive than in EGFP-negative UBCs

We had previously shown that the GIRK current in UBCs is heavily regulated by activation of group II mGluRs [11]. Thus, we tested whether potassium current modulation by group 2 mGluRs is detectable in both the UBC subtypes. As expected, in whole-cell configuration, the current of EGFP-negative cells was strongly increased (by  $109.5 \pm 32.6$  %,  $n=4$ ) by the broad spectrum mGluR agonist t-ACPD (100 μM); surprisingly, however, the current of the EGFP-positive cells was not affected (the current in t-ACPD decreased by  $0.2 \pm 3.3$  %; six cells, Fig. 9). This was unexpected because we had also suggested that group II mGluRs are expressed in both UBC subclasses. Therefore, we performed additional experiments in which EGFP-positive UBCs were recorded in the cell-attached configuration, which preserves intact all intracellular pathways. Notably, all (eight of eight) of the EGFP-positive cells measured showed a strong response to application of the group II mGluR agonist APDC (10 μM), which completely abolished intrinsic firing in control conditions and after it was stimulated by activation of group I mGluRs with DHPG (Fig. 10), thus confirming that both UBC subclasses express group II mGluRs, although the coupling with ion channels appears to be mediated

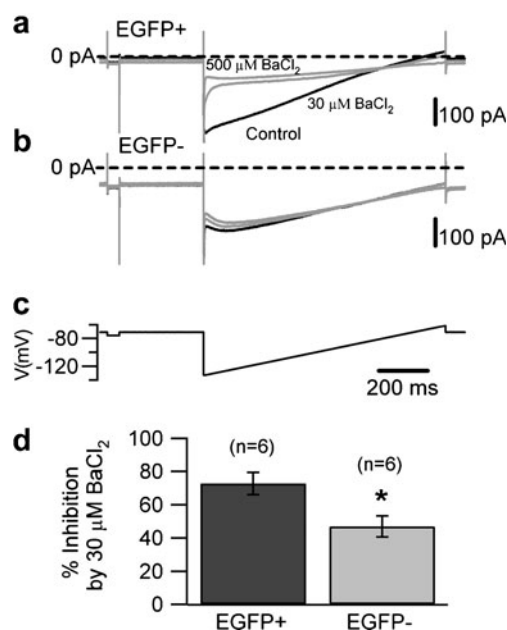


**Fig. 8** Background currents have different properties in the two UBC subtypes. **a, b** Whole-cell recordings of background potassium currents in control condition (*black traces*) and in the presence of 30 and 500 μM BaCl<sub>2</sub> (*gray traces*) in an EGFP-positive (**a**) and an EGFP-negative UBC (**b**). **c, d** The currents were obtained in response to a slow voltage ramp (**c** from -140 to -65 mV, 1 second duration). The bar chart in **d** compares the fractional block induced by 30 μM BaCl<sub>2</sub> in EGFP-positive and EGFP-negative UBCs. Fractional block was calculated assuming that 500 μM BaCl<sub>2</sub> blocks 100 % of the barium-sensitive current

by pathways that, contrary to the EGFP-negative cells, are sensitive to intracellular dialysis.

Because GIRK channels can be coupled to GABA<sub>B</sub> receptors, we tested whether this was also the case in UBCs. In whole-cell recordings, neither the GABA<sub>B</sub> agonist baclofen (50 μM) nor the antagonist CGP55845 (2 μM) had any significant effect on the current of EGFP-positive cells (when data from all six recorded cells were pooled together; data not shown). However, in one of six EGFP-positive cells, a clean, reversible, effect of baclofen was detected. This observation could have two main explanations: (a) a cellular heterogeneity within the EGFP-positive UBC population and (b) a current rundown due to the intracellular dialysis in whole-cell configuration. To solve this riddle, we performed cell-attached recordings to maintain intact the intracellular milieu. In this configuration, all (six of six) EGFP-positive cells showed a clear response to baclofen, which reversibly reduced or stopped intrinsic firing (Fig. 11a), while none of the tested EGFP-negative cells responded to baclofen (Fig. 11b;  $n=5$ ).

These data show that background potassium currents, most likely mediated by KCNJ subunits, differ in their size and modulation between the two UBC subtypes. We hypothesized that this difference could be correlated with the



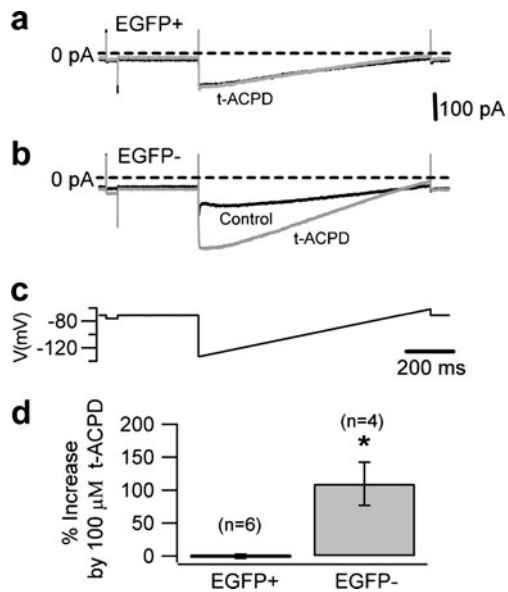


**Fig. 9** Metabotropic glutamate receptors differentially modulate the whole-cell background potassium currents in UBCs. **a** Whole-cell recording of the background potassium current in EGFP-positive UBCs in control conditions (*black traces*) and in the presence of 100  $\mu$ M t-ACPD (*gray traces*). The whole-cell current in EGFP-positive UBCs was not affected by 100  $\mu$ M t-ACPD. **b** Bath application of 100  $\mu$ M t-ACPD increased the background potassium current in EGFP-negative UBCs by 109.5 $\pm$ 32.6 % compared to control (at  $-120$  mV). The background potassium currents were recorded in response to a slow voltage ramp from  $-140$  to  $-65$  mV for 1 s (**c**)

type of KCNJ subunit expressed in the two cell types. In sections labeled by antibody to GIRK2 (KCNJ6), granule cells and glomeruli were distinctly immunostained (Fig. 12a). Upon close inspection of lobules X and IX,

however, several UBC somata and brushes appeared more prominently labeled than granule cells (Fig. 12b, c). The GIRK2-labeled UBCs matched the CR+ UBC in distribution (compare Fig. 1c with Fig. 12a). Double immunostaining and confocal imaging showed that only one out of 689 CR+ UBCs ( $N=3$  mice) lacked GIRK2 immunolabeling. All GIRK2-positive UBC were CR+ (Fig. 12d–i), whereas mGluR1 $\alpha$ + (EGFP-positive) UBCs were unlabeled (Fig. 12j–l). Thus, the dialysis-resistant coupling of the UBC background current to group II mGluR appears correlated with the expression of the GIRK2 subunit, as this is only expressed in EGFP-negative cells, while the dialysis-sensitive coupling to both GABAB and group 2 mGluRs is probably correlated with the expression of some other still unidentified channel subunit.

## Discussion

We performed immunocytochemical studies and whole-cell patch clamp recordings in lobules IX and X of slices from transgenic mice in which EGFP expression linked to the *Grp* promoter allows the identification of mGluR1 $\alpha$ + UBCs. Our morphological data confirm the differential distribution of mGluR1 $\alpha$ + vs. CR+ UBCs in the GENSAT Tg (Grp-EGFP) mice and demonstrate that CR+ (EGFP-negative) and mGluR1 $\alpha$ + (EGFP-positive) UBCs differ significantly in cell body size. Moreover, our electrophysiological data show that these two UBC populations also differ with regard to input resistance,  $I_h$  expression, firing phenotype, and in the size and pharmacological profile of the background potassium conductance (summarized in Table 1), supporting

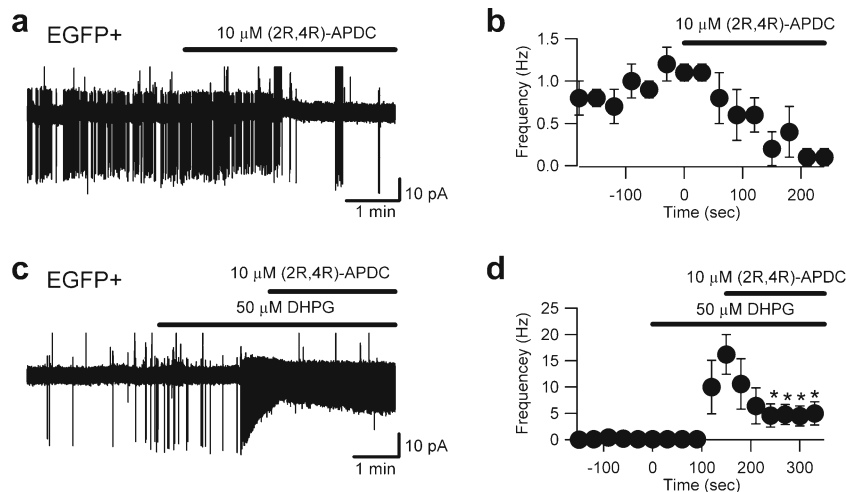
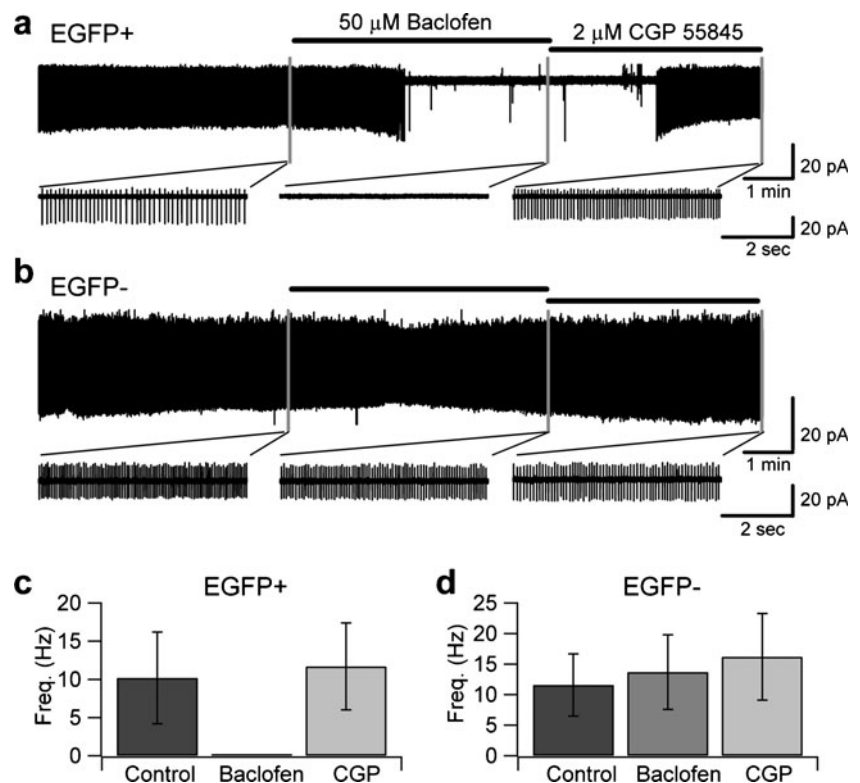


**Fig. 10** Cell-attached recordings reveal a group II mGluR-dependent modulation of EGFP-positive UBC firing. **a** Cell-attached recording from an EGFP-positive UBC in control conditions and in the presence of the group II mGluR agonist (2R,4R) APDC (*bar above the trace*); note that APDC almost completely abolished intrinsic firing. The graph in **b** reports pooled data from four cells. In order to test the

effect of group II mGluR activation in many EGFP-positive UBCs that show little or no spontaneous activity, the cells were first stimulated with DHPG and then APDC was co-applied (**c**). **d** Data pooled from four such experiments and shows that APDC significantly reduced the increase in firing frequency elicited by DHPG

**Fig. 11** GABA<sub>B</sub> receptor activation modulates background potassium currents in EGFP-positive, but not in EGFP-negative UBCs. **a** Voltage-clamp recordings of intrinsically firing EGFP-positive UBCs in cell-attached configuration. Bath application of 50  $\mu$ M baclofen, a GABA<sub>B</sub> agonist, hyperpolarized EGFP-positive UBCs and stopped intrinsic firing. The baclofen effect was reversed by washout with ACSF including 2  $\mu$ M CGP 55845. In 2  $\mu$ M CGP 55845, intrinsic firing of EGFP-positive UBCs was unaltered compared to the control condition. **b** Intrinsic firing of EGFP-negative UBCs was not affected by bath application of baclofen and CGP 55845



the notion of a profound diversity between the two UBC populations. This notion is further supported by multivariate statistical analysis performed on the whole set of recorded UBCs using four variables (specific membrane resistance, capacitance, inter-spike interval ratio, and coefficient of variation of firing; Fig. 13). Both principal component and cluster analysis show an almost perfect separation of EGFP-negative and EGFP-positive UBCs, supporting the idea that they identify two separate neuronal populations. Notably the few points that seem misplaced all represent EGFP-negative neurons, suggesting that they may have been mGluR1 $\alpha$ + UBCs in which EGFP expression was too low to be detected.

As our electrophysiological measurements were performed on both homozygous and heterozygous Tg(Grp-EGFP) mice and thus the subset of EGFP-negative UBCs might have included some mGluR1 $\alpha$ + UBCs (expressing EGFP below detection level) in addition to CR+ UBCs, the cell subclass-specific functional differences between UBCs may actually be even larger than we observed. Indeed, Fig. 13 suggests that a few (three to four) EGFP-negative cells might have been mGluR1 $\alpha$ + UBCs in which EGFP expression was below detection; if these cells were removed from the average data, the differences between the two classes would be even stronger. Additionally, the known relationship between size of the neuronal somatodendritic compartment and the axonal volume and axonal branching [22, 23] suggests that mGluR1 $\alpha$ + UBCs and CR+ UBCs may also differ with regard to the divergence of their outputs.

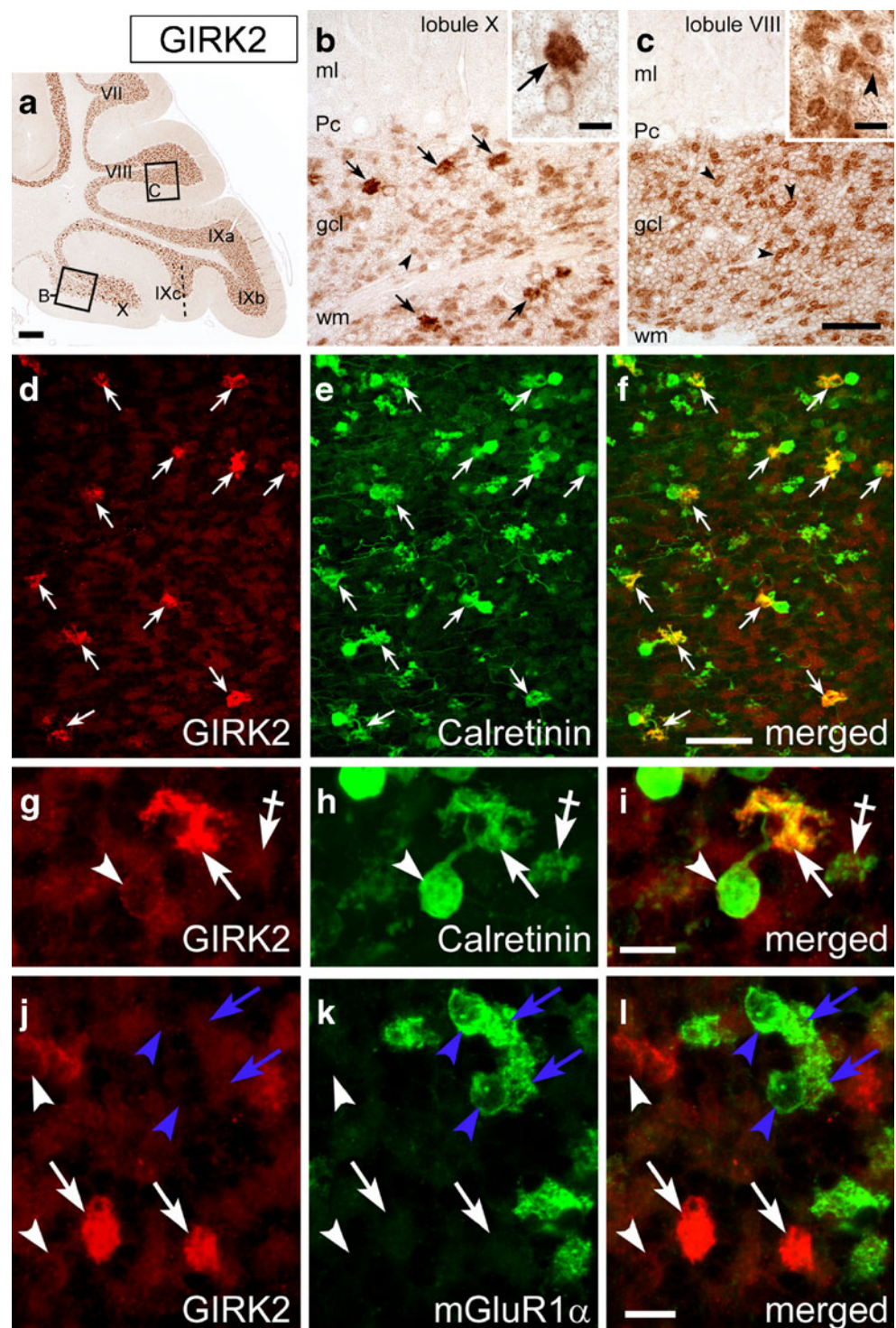
#### Distinct Subpopulation Properties May Help Reconcile Previous Findings

While the capacitance value in UBCs was always larger than in granule cells, it differed significantly between the two UBC subpopulations. This observation may help reconcile some of the differences in UBC firing phenotypes that were previously reported. Diana et al. [12] described rat UBCs as bursting neurons with capacitance between 8 and 15 pF (the same group previously reported capacitance values between 10 and 20 pF, [24]), while Russo et al. [10] described murine UBCs as intrinsically firing, non adapting neurons with capacitance of  $23 \pm 1$  pF.

In the present study, we show that EGFP-negative UBCs, which by and large correspond to the CR+ UBCs, have capacitance of  $20.2 \pm 0.7$  pF (similar to the  $23 \pm 1$  pF,  $p > 0.05$ ), while the EGFP-positive UBCs, which represents a substantial proportion of the mGluR1 $\alpha$ + UBCs, have capacitance of  $16.6 \pm 0.6$  pF. Thus, it is reasonable to propose that the differences between the results from the two groups of investigators are, at least in part, the consequence of a cell selection bias leading each group to study almost exclusively cells belonging to only one of the subtypes, although differences in factors such as recording temperature, animal age, or species may also contribute. The hypothesis that the two labs focused on different UBC subpopulations is further supported by the observation that, in the present study, the firing pattern of EGFP-negative UBCs



**Fig. 12** The brushes of CR+ UBCs are intensely labeled by GIRK2 antibody. **a–c** Images from deparaffinized, DAB immunoreacted parasagittal sections of wild-type mouse cerebellum. At low magnification GIRK2 immunoperoxidase labeling is evenly localized to the granular layer across the cerebellar lobules. In addition, the granular layer of folium IXc and lobule X contains GIRK2-positive UBCs, whose brushes are much more intensely labeled than the parent cell bodies. (*arrows in b and inset b*). Granule cells are much less intensely anti-GIRK2 immunoreactive in lobule X and folium IXc (compare **b** to **c**) than in other vermal lobules. **b, c** Boxed areas from **a**. *ml* molecular layer, *Pc* Purkinje cell layer, *wm* white matter. **d–i** Confocal immunofluorescence images from cerebellar cryosections of wild-type (**d–i**) and Tg(Grp-EGFP) mice (**j–l**). Intense GIRK2 immunoreactivity is present in the brushes (*white arrows*) of CR+ UBCs (*white arrowheads* indicate UBCs cell bodies). By contrast, mGluR1 $\alpha$ + UBCs are at background level (*blue arrowheads and arrows in j–l*). *Crossed arrows in g–i* point to a CR+/GIRK2-negative mossy fiber terminal. *Scale bars: a* 200  $\mu$ m, **b–f** 50  $\mu$ m, **g–l**, and *insets in b, c* 10  $\mu$ m



closely resemble that described by Russo et al. [10, 11], while the EGFP-positive UBCs showed more irregular, burst-like, firing reminiscent of that described by Diana et al. [12]. The similarity of the present results with those obtained in wild-type CD-1 mice by Russo et al. [10, 11] also suggests that the potential effects, if any, of the EGFP-transgene expression on the cell size and electrophysiological properties are negligible.

#### Modulation of Background Potassium Current Is Cell-Type Specific

Potassium channels mediate a large fraction of the background current in UBCs. Expression of GIRK currents within the UBC population had been reported previously, albeit without definition of the UBC subclasses. Knoflach and Kemp [25] described G-protein-coupled inwardly rectifying potassium



**Table 1** Synopsis of UBC properties

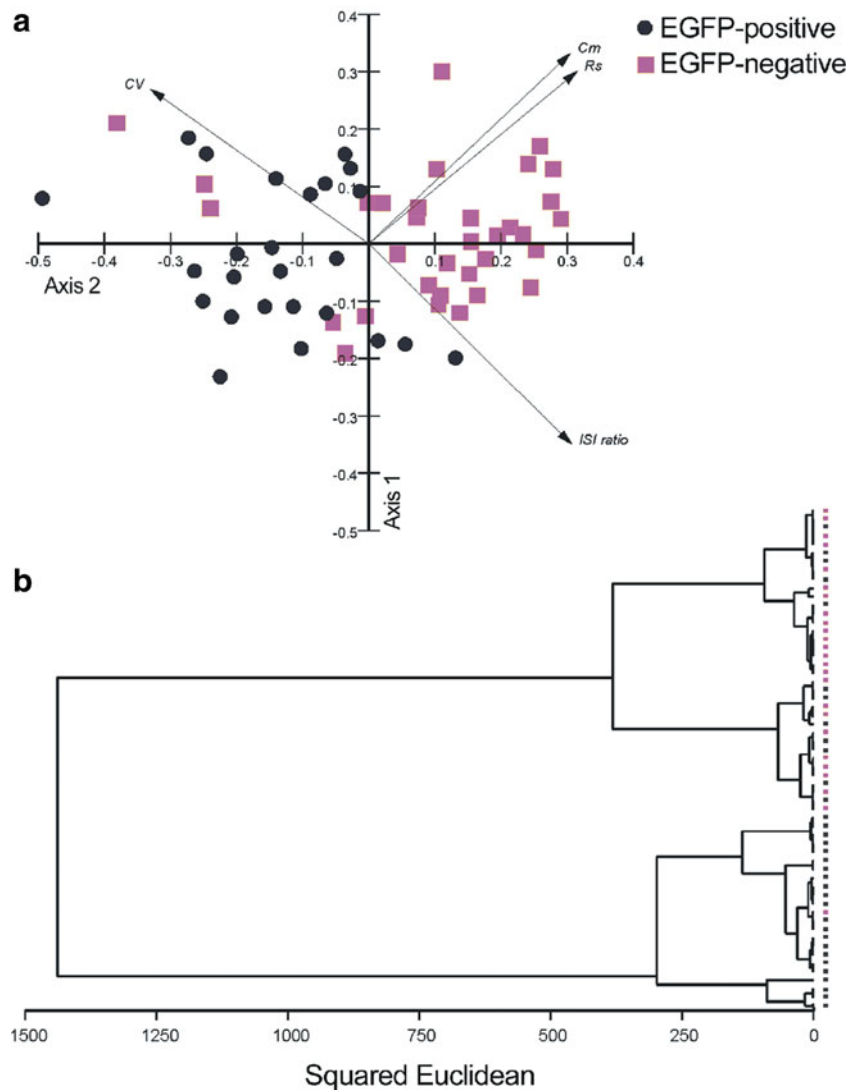
UBC subset	Size ( $\mu\text{m}^2$ )	Cap (pF)	Rm ( $\text{k}\Omega \text{cm}^2$ )	Intrinsic firing (%)	ISI ratio (wcr)	Firing CV (wcr)	Modulation
EGFP-positive (mGluR1 $\alpha$ +) ( $n=250$ )	48.3 $\pm$ 0.4	16.6 $\pm$ 0.7	6.4 $\pm$ 0.5	49.1 (c-att.) 37.3 (wcr)	0.3 $\pm$ 0.1 ( $n=18$ )	1.07 $\pm$ 0.20 ( $n=18$ )	Group II mGluR GABA <sub>B</sub> (c-att. only)
EGFP-negative (calretinin+) ( $n=250$ )	63.2 $\pm$ 0.6	20.2 $\pm$ 0.7	13.7 $\pm$ 0.9	87.5 (c-att.) 85.0 (wcr)	0.56 $\pm$ 0.04 ( $n=30$ )	0.45 $\pm$ 0.08 ( $n=31$ )	Group II mGluR (wcr)

*c-att.* cell-attached recording, *wcr* whole-cell recording

currents sensitive to the group II mGluR agonists DCG-IV and LY354740 in acutely dissociated UBCs. GIRK2 immunoreactivity in CR<sup>+</sup> UBCs, validated by lack of expression in *Girk2* knockout mice, was further shown in a Down syndrome mouse model by Harashima et al. [26]; moreover, Aguado et al. [27] reported that virtually all the UBCs that express GIRK2 also express GIRK3. Additionally, Russo et

al. [11] showed that GIRK channel modulation through group II metabotropic glutamate receptors regulates the firing phenotype in UBCs (most likely CR<sup>+</sup>). Our immunocytochemical analysis shows that expression of GIRK2 was only detectable in CR<sup>+</sup> (EGFP-negative) UBCs, whose current was sensitive to modulation by group II mGluR. This finding suggests that the GIRK2 subunit provides most of the

**Fig. 13** Multivariate analysis confirms the existence of two distinct populations of UBCs. **a** Principal component analysis of four variables obtained from recorded UBCs. The variables were capacitance, specific membrane resistance, spike coefficient of variation (in cell-attached) and inter-spike interval ratio (in cell-attached). The two axes accounted for 80 % of the variance in the sample. The eigenvector loadings of the variables were 0.485, 0.502, -0.525, and 0.488 on the first and 0.528, 0.479, 0.428, and -0.556 for the second axis, respectively. Note that EGFP-positive and EGFP-negative UBCs form two clouds with minimal contamination. Notably, all the three major outliers (*three squares in the second quadrant*) were EGFP-negative cells, suggesting that they may represent false negatives in which the EGFP expression was below detection. **b** Cluster analysis on the same data set also shows two main clusters, one formed by EGFP-positive and the other by EGFP-negative UBCs



background current in EGFP-negative UBCs and is selectively modulated in a cell dialysis-resistant manner by group II mGluR. Interestingly, in the *weaver* mouse *KCNJ6*—the gene coding for GIRK2—undergoes an amino acid substitution in the pore-forming region that results in the loss of GIRK2 currents; the mutation leads to degeneration of granule cells in the median cerebellum and dopaminergic neurons in the substantia nigra pars compacta [28, 29]. Consequently, the apparent lack of GIRK2 expression in the mGluR1 $\alpha$ + UBCs may suggest that this UBC subclass would be spared in homozygous *weaver* mutant mice, whereas most CR+ UBCs might undergo cell death.

In keeping with the idea that the group II mGluR modulation observed in whole-cell recordings is selective for GIRK2-containing channels, the potassium current in the mGluR1 $\alpha$ + UBCs was insensitive to group II mGluR activation in this configuration. However, in cell-attached configuration, in which the intracellular pathways are intact, the firing of EGFP-positive UBCs, which do not express GIRK2, was down-modulated both by group II mGluR and GABA<sub>B</sub> receptor activation, suggesting the activation of an inhibitory current, most likely carried by potassium ions. GABA<sub>B</sub> modulation, on the contrary, was not observed in EGFP-negative cells, suggesting that GIRK2 channels are not coupled to GABA<sub>B</sub> in UBCs. However, this selective coupling does not represent general rule because GIRK2-mediated currents are activated by GABA<sub>B</sub> in neurons of the substantia nigra [30].

A final consideration concerns the pathways involved in mGluR and GABA<sub>B</sub> signaling in EGFP-positive UBCs. In whole-cell recordings, GABA<sub>B</sub> activation had detectable effects in only one of six cells, and no effect of mGluRs was detected; however, all of the EGFP-positive cells recorded in cell-attached were modulated by activation of these metabotropic receptors. This result was unexpected because activation of GIRK channels is thought to be mediated by direct binding of G $\beta\gamma$  dimers to the channels [31, 32] and therefore should withstand intracellular dialysis. Thus, our data may suggest an unusual coupling between the metabotropic receptors and the GIRK channels in UBCs. More studies will be needed to identify the pathways involved in this still undefined signaling cascade.

#### Diverse Electrophysiological Properties Suggest Peculiar Roles of UBC Subpopulations

Intrinsically firing cells provide fine output modulation in response to diverse inputs. In particular, EGFP-negative UBCs, which according to our immunohistochemical data are in large part CR+, show a nearly monotonic input/output function over a relatively large input range [10]. Thus, such cells, while amplifying the vestibular input as a consequence of their divergent synapses onto their postsynaptic targets, provide a fine-tuned amplification that follows almost

linearly the input properties. Bursting neurons, such as the EGFP-positive UBCs, on the other hand, may be ideally suited to act as supra-linear signal amplifiers because any input large enough to cross threshold will lead to a burst of action potentials, thus enhancing the signal downstream.

Moreover, a bursting phenotype allows temporal separation and possibly also organization of temporally randomly distributed inputs, as action potential bursts may lead to inactivation of sodium channels and activation of calcium-dependent potassium channels, creating a refractory period at the end of the burst and leading to clear temporal segregation of inputs. The fact that the presence of CR+ UBCs is by and large limited to a relatively well-defined portion of the mouse cerebellum (lobule X and IXc; Fig. 1) is intriguing and suggests a selective function of these cells in cerebellar circuitries. Possible correlations between this function and a specific connectivity or any other functional and/or morphological property of this particular cerebellar area remain to be assessed. Whereas it has been demonstrated that primary vestibular fibers innervate CR+ UBCs [3], the inputs of mGluR1 $\alpha$ + UBCs remain to be established. The differential modulation of the background current suggests that the inputs to the two cell populations may also differ. Moreover, the divergence and mode of distribution of the axons originating from the smaller mGluR1 $\alpha$ + UBCs and the larger CR+ UBCs are still unknown.

An additional step in the elucidation of the function of cerebellar UBCs will therefore require a more detailed study of their synaptic properties to determine whether the two UBC subpopulations share the same inputs and show any type of synaptic plasticity and the extent by which the differences between their somatodendritic compartments extend to their axonal compartments.

In conclusion, morphological, immunocytochemical, and electrophysiological data cumulatively provide a strong body of evidence suggesting that the mGluR1 $\alpha$ + and the CR+ UBC subpopulations perform different functions in the cerebellar microcircuits.

**Acknowledgments** This work was supported by NIH grant RO1 09904. Paraffin embedding and sectioning of the paraffin-embedded blocks was performed by Northwestern University Mouse Histology and Phenotyping Laboratory, which is supported by a Cancer Center Support Grant (NCI CA060553). The authors wish to thank Drs. Joe P. Doyle, Joseph D. Dougherty, and Nataniel Heintz, The Rockefeller University, New York, NY, for breeding pairs of Tg(Grp-EGFP)DV197 mice.

**Conflict of Interest** No conflict of interest exists for any of the authors.

#### References

1. Nunzi MG, Shigemoto R, Mugnaini E. Differential expression of calretinin and metabotropic glutamate receptor mGluR1alpha

- defines subsets of unipolar brush cells in mouse cerebellum. *J Comp Neurol.* 2002;451:189–99.
2. Mugnaini E, Sekerková G, Martina M. The unipolar brush cell: a remarkable neuron finally receiving deserved attention. *Brain Res Rev.* 2010;66:220–45.
  3. Diño MR, Perachio AA, Mugnaini E. Cerebellar unipolar brush cells are targets of primary vestibular afferents: an experimental study in the gerbil. *Exp Brain Res.* 2001;140:162–70.
  4. Jaarsma D, Diño MR, Cozzari C, Mugnaini E. Cerebellar choline acetyltransferase positive mossy fibres and their granule and unipolar brush cell targets: a model for central cholinergic nicotinic neurotransmission. *J Neurocytol.* 1996;25:829–42.
  5. Nunzi MG, Russo M, Mugnaini E. Vesicular glutamate transporters VGLUT1 and VGLUT2 define two subsets of unipolar brush cells in organotypic cultures of mouse vestibulocerebellum. *Neuroscience.* 2003;122:359–71.
  6. Nunzi MG, Mugnaini E. Aspects of the neuroendocrine cerebellum: expression of secretogranin II, chromogranin A and chromogranin B in mouse cerebellar unipolar brush cells. *Neuroscience.* 2009;162:673–87.
  7. Sekerková G, Ilijic E, Mugnaini E. Time of origin of unipolar brush cells in the rat cerebellum as observed by prenatal bromodeoxyuridine labeling. *Neuroscience.* 2004;127:845–58.
  8. Dieudonné S. Submillisecond kinetics and low efficacy of parallel fibre-Golgi cell synaptic currents in the rat cerebellum. *J Physiol.* 1998;510(Pt 3):845–66.
  9. Forti L, Cesana E, Mapelli J, D'Angelo E. Ionic mechanisms of autorhythmic firing in rat cerebellar Golgi cells. *J Physiol.* 2006;574:711–29.
  10. Russo MJ, Mugnaini E, Martina M. Intrinsic properties and mechanisms of spontaneous firing in mouse cerebellar unipolar brush cells. *J Physiol.* 2007;581:709–24.
  11. Russo MJ, Yau HJ, Nunzi MG, Mugnaini E, Martina M. Dynamic metabotropic control of intrinsic firing in cerebellar unipolar brush cells. *J Neurophysiol.* 2008;100:3351–60.
  12. Diana MA, Otsu Y, Maton G, Collin T, Chat M, Dieudonné S. T-type and L-type Ca<sup>2+</sup> conductances define and encode the bimodal firing pattern of vestibulocerebellar unipolar brush cells. *J Neurosci.* 2007;27:3823–38.
  13. Ruigrok TJ, Hensbroek RA, Simpson JI. Spontaneous activity signatures of morphologically identified interneurons in the vestibulocerebellum. *J Neurosci.* 2011;31:712–24.
  14. Simpson JI, Hulscher HC, Sabel-Goedknecht E, Ruigrok TJ. Between in and out: linking morphology and physiology of cerebellar cortical interneurons. *Prog Brain Res.* 2005;148:329–40.
  15. Doyle JP, Dougherty JD, Heiman M, Schmidt EF, Stevens TR, Ma G, et al. Application of a translational profiling approach for the comparative analysis of CNS cell types. *Cell.* 2008;135:749–62. Erratum in: *Cell* 2009;139:1022.
  16. Gong S, Zheng C, Doughty ML, Losos K, Didkovsky N, Schambra UB, et al. A gene expression atlas of the central nervous system based on bacterial artificial chromosomes. *Nature.* 2003;425:917–25.
  17. Pearson K. On lines and places of closest fit to systems of points in space. *Phil Mag.* 1901;2:559–72.
  18. Diño MR, Willard FH, Mugnaini E. Distribution of unipolar brush cells and other calretinin immunoreactive components in the mammalian cerebellar cortex. *J Neurocytol.* 1999;28:99–123.
  19. Floris A, Diño M, Jacobowitz DM, Mugnaini E. The unipolar brush cells of the rat cerebellar cortex and cochlear nucleus are calretinin-positive: a study by light and electron microscopic immunocytochemistry. *Anat Embryol (Berl).* 1994;189:495–520.
  20. Diño MR, Mugnaini E. Distribution and phenotypes of unipolar brush cells in relation to the granule cell system of the rat cochlear nucleus. *Neuroscience.* 2008;154:29–50.
  21. Englund C, Kowalczyk T, Daza RA, Dagan A, Lau C, Rose MF, et al. Unipolar brush cells of the cerebellum are produced in the rhombic lip and migrate through developing white matter. *J Neurosci.* 2006;26:9184–95.
  22. Chklovskii DB. Synaptic connectivity and neuronal morphology: two sides of the same coin. *Neuron.* 2004;43:609–17.
  23. Peters A, Palay S, Webster dF. The fine structure of the nervous system: the neurons and supporting cells. Philadelphia: Saunders; 1976.
  24. Dugué GP, Dumoulin A, Triller A, Dieudonné S. Target-dependent use of co-released inhibitory transmitters at central synapses. *J Neurosci.* 2005;25:6490–8.
  25. Knoflach F, Kemp JA. Metabotropic glutamate group II receptors activate a G protein-coupled inwardly rectifying K<sup>+</sup> current in neurones of the rat cerebellum. *J Physiol.* 1998;509(Pt 2):347–54.
  26. Harashima C, Jacobowitz DM, Stoffel M, Chakrabarti L, Haydar TF, Siarey RJ, et al. Elevated expression of the G-protein-activated inwardly rectifying potassium channel 2 (GIRK2) in cerebellar unipolar brush cells of a Down syndrome mouse model. *Cell Mol Neurobiol.* 2006;26:719–34.
  27. Aguado C, Colón J, Ciruela F, Schlaudraff F, Cabañero MJ, Perry C, et al. Cell type-specific subunit composition of G protein-gated potassium channels in the cerebellum. *J Neurochem.* 2008;105:497–511.
  28. Patil N, Cox DR, Bhat D, Faham M, Myers RM, Peterson AS. A potassium channel mutation in weaver mice implicates membrane excitability in granule cell differentiation. *Nat Genet.* 1995;11:126–9.
  29. Surmeier DJ, Mermelstein PG, Goldowitz D. The weaver mutation of GIRK2 results in a loss of inwardly rectifying K<sup>+</sup> current in cerebellar granule cells. *Proc Natl Acad Sci USA.* 1996;93:11191–5.
  30. Koyrakh L, Luján R, Colón J, Karschin C, Kurachi Y, Karschin A, et al. Molecular and cellular diversity of neuronal G-protein-gated potassium channels. *J Neurosci.* 2005;25:11468–78.
  31. Misgeld U, Bijak M, Jarolimek W. A physiological role for GABAB receptors and the effects of baclofen in the mammalian central nervous system. *Prog Neurobiol.* 1995;46:423–62.
  32. Reuveny E, Slesinger PA, Inglese J, Morales JM, Iniguez-Lluhi JA, Lefkowitz RJ, et al. Activation of the cloned muscarinic potassium channel by G protein beta gamma subunits. *Nature.* 1994;370:143–6.